Theoretical Population Biology 80 (2011) 49–63

Contents lists available at ScienceDirect

Theoretical Population Biology

journal homepage: www.elsevier.com/locate/tpb

Dynamic modeling of cooperative protein secretion in microorganism populations

Yuval Elhanati [a,b,*], Stefan Schuster [c], Naama Brenner [a,d,*]

[a] Laboratory of Network Biology Research, Technion — Israel Institute of Technology, Haifa, Israel

[b] Department of Physics, Technion — Israel Institute of Technology, Haifa, Israel

[c] Department of Bioinformatics, School of Biology and Pharmaceutics, Friedrich Schiller University of Jena, Jena, Germany

[d] Department of Chemical Engineering, Technion — Israel Institute of Technology, Haifa, Israel

ARTICLE INFO

Article history:
Received 12 October 2010
Available online 12 April 2011

Keywords:
Microorganisms
Population dynamics
Nonlinear dynamical systems
Protein secretion
Cooperation

ABSTRACT

Interactions between microorganisms can have a crucial effect on their population dynamics. Typically, interactions are mediated through the environment by molecules and proteins that are products of cell metabolism and physiology; they therefore reflect the internal dynamics of the single cell. In this work we aim to integrate single-cell properties of gene expression that affect indirect interactions between microorganisms under challenging conditions, into a quantitative model of population dynamics. Specifically we address the problem of a microbial population secreting a protein that can actively extract a growth-limiting resource, such as a simple sugar or iron, from the environment. The genes coding for the protein can undergo random epigenetic transitions between active and silenced states, and can be repressed by the product of their reaction. We model cooperative and competitive interactions between protein producing and non-producing phenotypes by nonlinear dynamical systems and analyze them both in terms of asymptotic states and of transient dynamics. Our model shows that phenotypic transitions allow a stable coexistence of the two phenotypes, and enables us to make predictions regarding the conditions required for such coexistence and the typical timescales of transient dynamics. It also shows how repression by the reaction product induces a feedback at the population-environment level that can result in limit cycle dynamics. The relation of these results to experiments are discussed.

1. Introduction

Individuals in a microbial population exhibit many forms of interaction. Typically they interact indirectly through the environment, for example by secreting and sensing of molecules. Even more indirectly, while competing for common essential resources, microorganisms can affect the environment and through it other members of the population by utilizing these resources with a varying degree of efficiency (Pfeiffer et al., 2001). All these interactions are mediated by products of cell metabolism and gene expression, and thus reflect the internal properties and dynamics of cell physiology. Therefore understanding a population of interacting individuals requires making a connection between the level of the single cell and that of the population. Here we aim to make this connection within a theoretical study of the population dynamics of microorganisms which face the task of active resource extraction from the environment, and interact through "public goods".

Public goods are beneficial resources affecting growth ("fitness") positively, whose production is costly to the individual but once produced they are publicly available. While the concept of public goods is an abstract and general one, in microorganism populations it is mostly associated with the expression and secretion of proteins with various functions (Crespi, 2001; West et al., 2006). Examples of such functions include the production of digestible carbon or iron from a hard-to-access substrate; construction of biofilms and multicellular structures; conflict with other microbes or the host immune system in the case of pathogens (Webb et al., 2003; Griffin et al., 2004; Parsek and Greenberg, 2005; Kreft, 2005; Modak et al., 2007; Diggle et al., 2007). In the present work we develop models inspired by the expression and secretion of molecules that extract a resource from the environment. Interactions between individuals in this case is considered "cooperative", since the production of the protein involves a metabolic cost which affects growth negatively, while the reaction products are generally available for uptake also by other neighboring cells and affect their growth positively (West and Buckling, 2003; Greig and Travisano, 2004; MacLean and Gudelj, 2006; Hauert et al., 2006;

* Corresponding authors at: Laboratory of Network Biology Research, Technion – Israel Institute of Technology, Haifa, Israel.

E-mail addresses: yuvalel@tx.technion.ac.il (Y. Elhanati), nbrenner@tx.technion.ac.il (N. Brenner).

0040-5809/$ – see front matter © 2011 Elsevier Inc. All rights reserved.
doi:10.1016/j.tpb.2011.03.005

MacLean, 2008; MacLean and Brandon, 2008; Gore et al., 2009; Jiricny et al., 2010; Schuster et al., 2010). Our goal in this study is to incorporate dynamic intracellular properties of the processes that create the interaction-mediating proteins, and to investigate how they are reflected in the population dynamics, both at asymptotic and at finite times.

We consider two dynamic effects on the expression of the protein mediating the interaction: phenotypic switching and feedback from the reaction product. The first, phenotypic switching, is inspired by the secretion of invertase to hydrolyze sucrose by yeast cells (Carlson and Botstein, 1982). The SUC genes of *S. Cerevisiae*, which code for invertase, are mostly located in sub-telomeric regions of the chromosome, making them sensitive to position-dependent random epigenetic transitions between active and silenced expression states with variable typical timescales of up to 15 generations (Gottschling et al., 1990; Louis, 1995; Vega-Palas et al., 2000). Such transitions render the individual phenotype unstable over time and can affect phenotypic coexistence, population variability and population dynamics.

The second dynamic effect is the repression of the resource-extracting protein by its own product in the environment. This effect is seen in at least two well-studied examples: invertase, which produces glucose from sucrose, is repressed by glucose in the medium in a manner typical of enzymes related to alternative carbon source metabolism (Gancedo, 1998); however here glucose is not introduced from the outside but is a result of the enzyme's own activity. This creates a negative feedback between gene expression at the single cell level, its effect on the environment and back on gene expression. A similar effect is found in bacterial siderophore expression (Kummerli et al., 2009). This second dynamic effect becomes important when cell density is large enough so that the reaction-product density is high.

Population dynamics in the presence of phenotypic switching, either random or environment-dependent, has been the subject of recent work in the context of antibiotic tolerance (Balaban et al., 2004; Kussell et al., 2005) and of time-varying environments (Lachmann and Jablonka, 1996; Thattai and van Oudenaarden, 2004; Kussell and Leibler, 2005; Wolf et al., 2005; Acar et al., 2008; Filiba et al., 0000). These situations describe challenging external conditions in which population heterogeneity, brought about by switching, can increase total fitness. The requirement for active extraction of an essential growth-limiting resource from the environment is another challenging situation in which cooperative interactions and heterogeneity can have consequences on population fitness and survival.

We develop a dynamical model to describe the indirect interactions between microorganisms through a common, growth-limiting resource in the environment, which is not supplied from the outside but instead is extracted by the microorganisms themselves. Our mathematical approach relies on continuous differential equations, enabling us to highlight the dynamic aspects of the problem in addition to its asymptotic stability properties. We define two regimes in which the two dynamic processes mentioned above — random epigenetic switching and repression by the product — dominate respectively, and study the population dynamics of competition and cooperation in each regime. We find that in a homogeneously mixed population, random switching between an expression state and a silenced state can support a stable coexistence between the two states if the switching rate is above a threshold. We also find an interesting decoupling between the dynamics of competition and cooperation of the phenotypes in the population on one hand, and the interaction of the total population with the environment on the other hand. In the presence of repression by the product, our results suggest the existence of limit cycle coexistence states. The role of variable gene expression is examined by considering the total population density, and in some cases an intermediate value of variability which maximizes this density is found. Finally we discuss suggestions for experimental tests of our predictions.

2. Model

2.1. Active resource extraction from the environment by a homogeneous population

First we present a model for a homogeneous population of microorganisms that secrete a resource-extracting protein. This will enable us to present the modeling framework and the basic underlying assumptions, which are also used in the subsequent models with a heterogeneous population.

Imagine a population of microorganisms secreting a protein into the environment. The protein is involved in a chemical reaction with an external substrate that results in a free concentration of a growth-limiting resource. The resource s governs the population growth rate through a sublinear monotonous function, such as the Monod function $\mu(s) = \mu_0 \frac{s}{s+k}$. Assuming that the biochemical reaction which produces the resource is rapid relative to gene expression and growth, we average over its dynamics and represent the amount of the reaction product — the growth-limiting resource — as directly depending on the population concentration u. The rate of resource generation $\dot{s}$ is therefore a function of this concentration u and of the available substrate in the environment. In a typical situation the amount of available substrate is limited, therefore a reasonable dependence on u is that of a Michaelis–Menten kinetics: $\dot{s} = c\frac{u}{u+z}$, or more generally an increasing and saturating function $g(u)$. The system of equations governing the dynamics of the two variables, population and resource concentrations, is then in dimensionless units:

$$\begin{aligned} \dot{u} &= u(\mu(s) - 1) \\ \dot{s} &= g(u) - d\mu(s)u, \end{aligned} \tag{1}$$

where time is normalized by the death rate and d is the inverse yield factor. Nontrivial fixed point solutions with nonzero (u^*, s^*) exist for this system if the condition $\mu(s^*) = 1$ can be satisfied, similar to a simple limiting-resource system. However because the resource is not supplied from outside but extracted by the population, an additional condition must be fulfilled, namely a positive balance between resource extraction and consumption ($d < 1$). (See Appendix A for derivation and analysis of the model).

2.2. Dynamics of exoenzyme expression: resource extraction with phenotypic switching

To model the dynamics of exoenzyme expression, we describe cells as being in one of two possible phenotypic states, coarsely representing gene expression states: a producing state, with population density u, and a non-producing state with respective density v. The well-mixed growth-limiting resource s now creates a homogeneous indirect interaction between the two phenotypic sub-populations. Producing cells grow at a rate smaller by a factor R ($R > 1$) at all values of s, representing the metabolic cost of exoenzyme production and secretion. Any effect that causes cells to switch between producing and non-producing states is described by transition rates $b_1(s), b_2(s)$ between them. Making several additional simplifying assumptions the equations in dimensionless units now take the form

$$\begin{cases} \dot{u} = (\mu(s) - 1)u - b_1(s)u + b_2(s)v \\ \dot{v} = (R\mu(s) - 1)v + b_1(s)u - b_2(s)v \\ \dot{s} = \dfrac{u}{u+1} - d(u+v)\mu(s). \end{cases} \tag{2}$$

(See Appendix B for details on the assumptions and non-dimensionalization.) The transition rates $b_1(s), b_2(s)$ can be constant or environment dependent (see below). If they vanish, $b_1 = b_2 = 0$, each phenotypic state is perfectly inherited by next generations and the model reduces to two distinct sub-populations. In this

case there cannot be stable population growth, and asymptotically there are only two possibilities: no population at all ($u = v = 0$ with an arbitrary value of s), or an unstable population consisting of only producing cells $\left(u = \frac{1}{d} - 1, v = 0, \mu(s) = 1\right)$. In this case, under invasion by non-producing cells, this population will evolve toward extinction since the extracted resource is essential for growth. If the resource is not essential but only beneficial for growth, $\mu(0) > 0$, the population will not become extinct but the non-producing sub-population will take over (see Appendix B). Much recent work has focused on this case of two completely stable phenotypes: Synthetic biology was used to realize this situation by creating two different genotypes by mutants which either constitutively express or not express the protein at all (Greig and Travisano, 2004; MacLean and Gudelj, 2006; Ross-Gillespie et al., 2007, 2009; Chuang et al., 2010).

In natural situations microorganisms do not maintain one expression state or another for infinite time nor with infinitely stable inheritance, and therefore the transition rates b_1, b_2 in the above model are generally nonzero. In the following sections we consider two special cases of the model that represent two dynamic properties of gene expression, random switching and repression by the reaction product, and study the resulting population dynamics.

3. Results

3.1. Random epigenetic transitions between active and silenced gene expression states

Yeast invertase can be secreted outside the cell and hydrolyze sucrose. It can be expressed by one of several genes in the SUC family (Carlson and Botstein, 1983). The position of most of these genes near the telomeres can result in cells slowly and randomly switching between an active and a silenced expression state (Gottschling et al., 1990; Louis, 1995; Vega-Palas et al., 2000). This instability is the primary dynamical aspect of invertase expression and secretion when cell density is low such that repression by the reaction product, glucose, does not play an important role. These transitions can, in principle, change the balance of cooperative and competitive interactions among microorganisms and affect the fixed points of the system qualitatively. Inspired by this system, we represent these transitions in our model by constant nonzero values of the transition rates, taken to be equal in both directions for simplicity. Analyzing the dynamical system (2) with $b_1 = b_2 = b$, we find that indeed it can support a single coexistence fixed point of the dynamics, where both cell states have nonzero concentrations (u^*, v^*, s^*) (see Appendix C). However this requires two conditions to be fulfilled:

$$d < \frac{1+R}{4} \tag{3}$$

$$b > B(R, d) \tag{4}$$

(see the definition of $B(R, d)$ in Appendix C). First, coexistence requires that resource consumption is not too high relative to its production. This condition comes about because the cells both produce and consume the resource. In contrast, if the resource were produced at a constant rate from the outside, the two competing sub-populations with switching between them would always maintain a stable coexistence state, even if consumption rate is very high (Filiba et al., 0000).

Second, coexistence requires the transition rate between phenotypes to be above a threshold determined by the other system parameters (R-selection coefficient, d-resource consumption). A plot of the threshold value of b is shown in Fig. 1. The threshold becomes very large near the line defined by the condition in (3), representing the limited region where coexistence can be achieved.

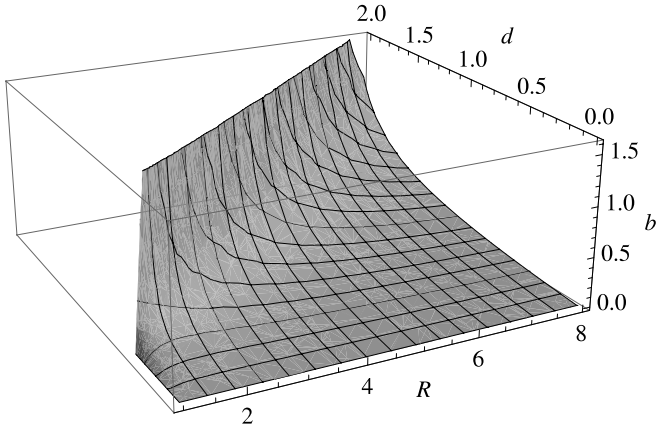

Fig. 1. Region of coexistence between producing and non-producing phenotypes in a population of microorganisms required to actively extract a resource from the environment. The shown manifold is a lower threshold on b, the transition rate between phenotypes, required for coexistence. It is plotted as function of R, selection coefficient, and d, resource consumption rate (see Eq. (2)).

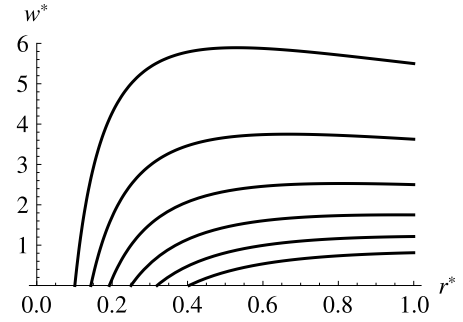

Fig. 2. Total population density as a function of the ratio of phenotypes at the coexistence fixed point. $R = 3.5$. Graphs are plotted for $d = 0.3$ (uppermost), $d = 0.4$, $d = 0.6$, $d = 0.8$ (lowermost). At a coexistence fixed point, r^* is never greater than 1 or smaller than the lower cutoff defined by the threshold Eq. (4), which depends on R and d. Notice that a higher value of the consumption rate d leads to an overall lower total population density.

At all values where the coexistence fixed point is physical (i.e. positive concentrations), it is stable. This can be proved using the Routh–Hurwitz conditions (see Appendix C.2). In addition to the coexistence state, the trivial fixed point extends to a continuum on the s axis. These states are stable only for $s < s^*$ where s^* is the value of the resource at the coexistence fixed point (see Appendix C.1).

At the stable coexistence fixed point, the population is characterized by the concentrations of the two phenotypes, u^*, v^*. Alternatively, it can be characterized by the total population density $w^* = u^* + v^*$, and the degree of heterogeneity in the population—for example the ratio between the two types, $r^* = u^*/v^*$. The ratio is in the region $0 < r < 1$, with $r = 1$ the maximally heterogeneous population where the two types appear in equal fractions. The coexistence fixed point defines a relation between these two variables:

$$w^*(r^*) = \frac{1}{d}\frac{r^*+R}{r^*+1} - \frac{r^*+1}{r^*}. \tag{5}$$

Fig. 2 illustrates this relation for different parameter values. It is seen that, for a fixed value of selection coefficient R, lower rates of consumption d result in higher total population density. For fixed (R, d), two different behaviors are seen regarding the dependence $w^*(r^*)$: either a monotonically increasing function, or an intermediate maximal value. By direct calculation the maximal

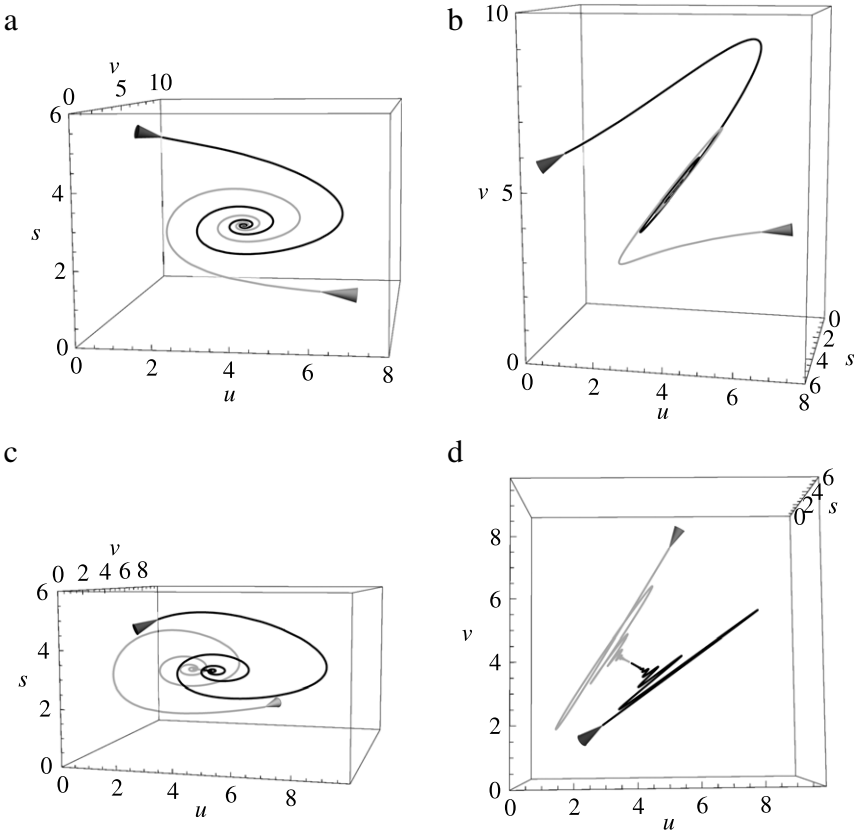

Fig. 3. Numerical trajectories of the dynamical system in Eq. (2) with different parameters and initial conditions in the phase space of (u, v, s), viewed from different angles (the cones indicate the initial conditions). The trajectories illustrate the decoupling of the phenotypic ratio dynamics from the total population dynamics in two characteristic cases: (a,b) (same two trajectories from different angles, parameters $b = 0.2$, $R = 1.1$, $d = 0.1$, $\mu_0 = 1.5$, $k = 1.5$). The ratio between phenotypes, producing and non-producing, is established rapidly and then a slower oscillatory relaxation occurs in the plane of fixed ratio, to the fixed point value of total population and resource. (c,d) (same two trajectories from different angles, parameters $b = 0.005$, $R = 1.001$, $d = 0.1$, $\mu_0 = 1.5$, $k = 1.5$) Fast oscillatory relaxation determines the total population and resource values, followed by a slower relaxation towards the fixed point value of the ratio.

value is obtained at

$$r^*_{\max} = \frac{\sqrt{d}}{\sqrt{R-1} - \sqrt{d}}. \tag{6}$$

When $R > 4d+1$, this maximum is obtained at an intermediate value of heterogeneity ($0 < r^*_{\max} < 1$), with a population density of

$$\max(w^*) = w^*(r^*_{\max}) = \frac{R}{d} - 2\sqrt{\frac{R-1}{d}}. \tag{7}$$

On the other hand when $R < 4d+1$, the above calculated value becomes $r^*_{\max} > 1$, which is outside the defined region of r^*. By tuning the transition rates b, either to the maximal value which gives the highest possible value of r (if $R < 4d + 1$) or to the intermediate value giving a maximum of w^* (if $R > 4d+1$), a level of heterogeneity at the coexistence fixed point can be obtained which maximizes population density.

We next consider the dynamics of trajectories approaching the fixed points. Numerical solutions of the equations indicate that convergence to the fixed point is sometimes oscillatory. Observing these oscillatory trajectories, it appears that the dynamics of the ratio between the two phenotypes is approximately independent of the dynamics of both the total population and the resource concentration. Examples are displayed in Fig. 3, showing trajectories in (u, v, s). The first pair of trajectories, with black and gray lines corresponding to different initial conditions, is shown in panels (a) and (b) from two points of view. These two trajectories are rapidly attracted to a plane on which the ratio between phenotypes is approximately constant, and then continue to oscillate in this plane until the total population and environment reach their fixed point values. On the other hand, the second pair of trajectories in panels (c) and (d), with different parameter values, features opposite dynamics: first damped oscillations approximately inside a plane of the initial ratio between phenotypes, and then a one dimensional convergence to the fixed point ratio. These observations motivate an approximation in which the dynamics of the ratio between phenotypes is decoupled from the dynamics of the total population and environment (which are strongly coupled to one another in both cases).

Defining new variables of phenotypic ratio $\left(r = \frac{u}{v}\right)$ and the total population ($w = u + v$), one may transform the equations (2) to the following equivalent system:

$$\begin{aligned} \dot{w} &= w\left(\frac{r+R}{r+1}\mu(s) - 1\right) \\ \dot{r} &= -\mu(s)(R-1)r - b(r^2-1) \\ \dot{s} &= \frac{w}{w+1+1/r} - \mathrm{d}\mu(s)w. \end{aligned} \tag{8}$$

The new equations have a simple interpretation. The total population w grows with an average rate $\mu_{\text{mean}} = \frac{r+R}{r+1}\mu(s)$ determined by its internal composition through the phenotypic ratio r. The dynamics of the ratio r is driven by two forces: the first is competition, tending to drive r toward zero. The second is the transitions, driving the ratio towards an equilibrium positive value (in this case of symmetric transition rates, this value is 1). Asymptotically r will tend to some value r^* between 0 and 1.

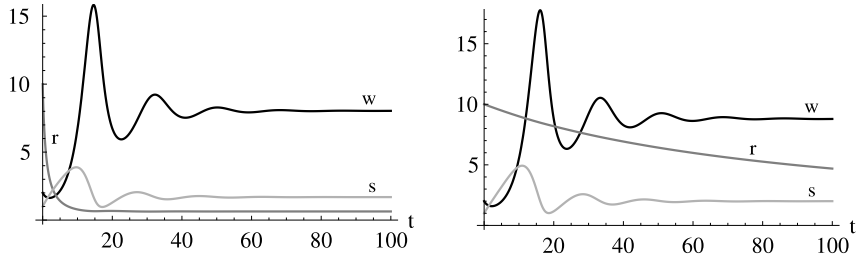

(a) $b = 0.1$ $R = 1.1$. (b) $b = 0.001$ $R = 1.001$.

Fig. 4. Total microorganism population (w), ratio between producing and non-producing phenotypes (r) and resource in the environment (s) as functions of time in the model for active resource extraction in the transformed variables, Eq. (8) (parameters: $d = 0.1$, $\mu_0 = 1.5$, $k = 1$).

The dynamics of r is independent of w, and depends on s only through $\mu(s)$, which is of limited dynamical range; therefore r is weakly coupled to the rest of the system, as our numerical analysis suggested. The equation for s shows that it is very weakly coupled to r, which only enters as an additive term in the denominator of the substrate production function, but strongly coupled to w.

Fig. 4 illustrates this decoupling in numerical solutions of the transformed equations with two sets of parameters. While the limiting resource s and the total population w exhibit strong coupled damped oscillations, the ratio r follows its own decaying trajectory, either faster or slower than the other two variables, with negligible traces of the oscillations.

We can solve the transformed system of equations in a decoupling approximation and identify the corresponding timescales (see Appendix D). In the leading order the typical time scale of ratio dynamics is

$$\tau_{\text{int}} = (4b^2 + (R-1)^2 \mu(\bar{s})^2)^{-\frac{1}{2}}, \tag{9}$$

where $\mu(\bar{s})$ is some characteristic value of the growth function. This approximation can be justified in one of two cases: either when s is changing very slowly while r is decaying rapidly, in which case $\bar{s}$ will be close to its initial value; or when s changes so rapidly that it had already decayed close to its fixed point value, in which case $\bar{s}$ will be that equilibrium value. τ_{int} is the *Internal Composition* relaxation time, the time it takes the system to reach a stable internal ratio between the two phenotypes, assuming decoupling. Now, keeping the decoupling assumption, if the changes in r are also not too great since it had already equilibrated or is changing very slowly, we can solve the reduced system:

$$\begin{aligned} \dot{w} &= w\left(\frac{\bar{r}+R}{\bar{r}+1}\mu(s) - 1\right) \\ \dot{s} &= \frac{w}{w+1+1/\bar{r}} - \mathrm{d}\mu(s)w. \end{aligned} \tag{10}$$

This reduces the problem back to a homogeneous population extracting the resource, Eq. (A.3), but with nonlinear functions - growth and extraction - depending parametrically on $\bar{r}$. The relaxation dynamics depends on the differences in slope between the production and consumption functions at the fixed point population value (see Appendix A). Except for the limiting case where these two slopes are very close to each other, the corresponding relaxation timescale towards the fixed point is found to be

$$\tau_{\text{env}} = (\mathrm{d}\mu'(s^*)w^*)^{-1}. \tag{11}$$

This is the *Environment* relaxation time, describing the process of equilibration between the total population and the environment. It is the same timescale found for a single population equilibrating with a growth-limiting resource in the environment and reaching its fixed point value regardless of the dynamics of this resource.

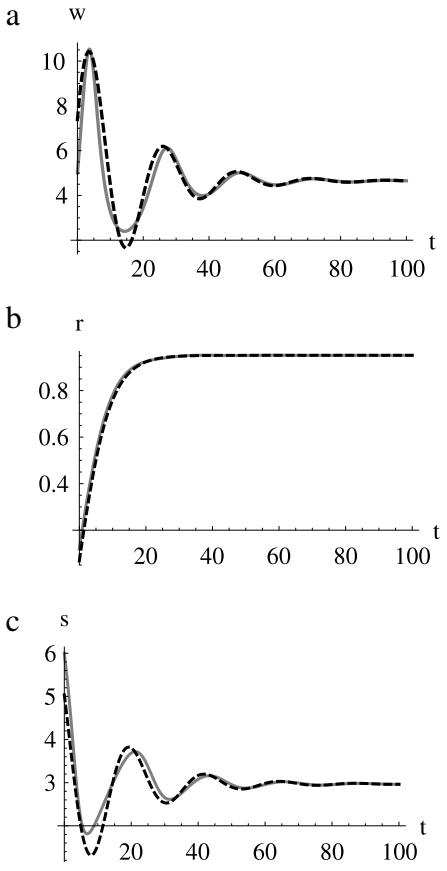

Fig. 5. Numerical solution (solid gray) and decoupling approximation (dashed black) for the model in transformed variables of total population and phenotype ratio, Eq. (8) (parameters: $b = 0.1$, $R = 1.1$, $d = 0.15$, $\mu_0 = 2$, $k = 3$).

This decoupling approximation is valid under conditions of timescale separation (see Appendix D). In practice we find numerically that sometimes it provides a good approximation to the dynamics even beyond the this strict validity regime. Fig. 5 illustrates the quality of the leading order solutions in the decoupling approximation. It displays the exact numeric solution of the full system (solid lines) along with the approximate analytic expression for r and an exponential approximation for w and s based on the calculated eigenvalues (dashed lines). Here there is a shorter timescale for the ratio dynamics (20 time units) than the timescale of the other variables (80 time units).

3.2. Negative feedback through the environment: modeling repression by the product

In several cases of active resource extraction, the phenotypic state is sensitive to the reaction product in the environment.

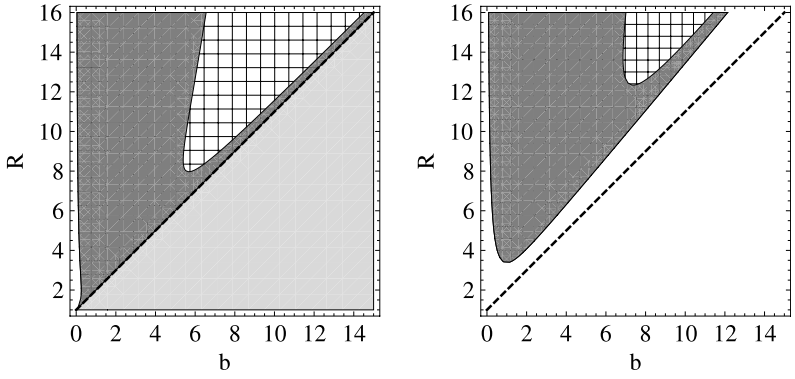

(a) $d = 0.65$. (b) $d = 1.2$.

Fig. 6. Stable states of the dynamics in a model with single-sided transitions $b_1 = 0$, $b_2 = b$, (in the region $s < s^0$) where transitions take place from the non-producing to the producing phenotype. Light gray: stable exclusion. Dark gray: stable coexistence. Checkered area: stable limit cycle. White area: no physical fixed points. Two values of d are shown. In both, $\mu'(s^*) = 1$.

Yeast production of invertase is repressed by glucose (Gancedo, 1998), which is a product of extracellular hydrolysis of sucrose by invertase; another example is bacterial production of the iron-scavenging molecule pyoverdin, which is repressed by the extracted iron (Kummerli et al., 2009). We model this effect by introducing a resource-dependent bias in the transition rates, $b(s)$. A simple such dependence is given by a step function as follows:

$$b_1(s) = \begin{cases} 0, & s < s^0 \\ b, & s > s^0 \end{cases}$$
$$b_2(s) = \begin{cases} b, & s < s^0 \\ 0, & s > s^0 \end{cases} \qquad (12)$$

where s^0 is the threshold resource concentration where the direction of transitions changes. Above this resource level transitions are solely to the non-producing state, and therefore after a transient all cells will be repressed; below the threshold there are transitions only to the producing state and thus the opposite situation will occur. Although this is a simplified description, it introduces the essential effect of a negative feedback from gene expression to the environment and back. More realistic smooth dependencies on the product level will be discussed below and will be shown to exhibit qualitatively similar behavior.

The Heaviside threshold in (12) allows an approximate analysis of the problem. Technically it defines two problems with one-way transitions (either $b_1 = 0$ or $b_2 = 0$) above and below a threshold value s^0; the sharp threshold allows us to analyze each of these subproblems with fixed transition rates separately. This analysis will hold for trajectories that stay entirely on one side of the threshold. We then discuss how these two regions are matched to obtain the behavior of trajectories that wander between the two regions.

Consider first the case where the resource level is above the threshold – $s > s^0$, $b_1(s) = b$ and $b_2(s) = 0$. Since transitions are only to the non-producing state, the fixed points are trivial ones located on the s axis. The axis is stable for $s < s_v = \mu^{-1}\left(\frac{1}{R}\right)$, and from that point onward, it is unstable. Therefore typical trajectories will be curved, repelling from the upper portion of the axis and converging to an attractive fixed point on the lower part (see Appendix E.1). If $s^0 > s_v$ there will be no stable fixed points above the threshold and trajectories will always eventually cross to the lower region of $s < s^0$, where transitions are only to producing cells.

The opposite case where the resource level is below the threshold – $s < s^0$, $b_1(s) = 0$ and $b_2(s) = b$, now enables a balance of transitions and competition effects between the two phenotypes. We used numerical sampling and analytical analysis to characterize the solutions in the entire parameter space (see Appendix E.2). The trivial points on the s axis are stable up to $s_u = \min\left(\mu^{-1}(1), \mu^{-1}\left(\frac{1+b}{R}\right)\right)$. (Note that $s_u > s_v$). In addition, three types of nontrivial fixed points are found: first, an exclusion fixed point, where the resource-extracting cells form a homogeneous population. Second, a fixed point with two viable sub-populations of nonzero density u^*, v^*. When this coexistence point is unstable, one sometimes find a stable limit cycle around it, in which the population composition cycles along time. For each set of parameters there is at most one stable state. Typical results on the $b - R$ plane for two values of d are displayed in Fig. 6, with different shading corresponding to different types of stable states – exclusion point, coexistence point and limit cycle. Whatever the stable state, if s^* is the resource value of the steady state (in the case of the limit cycles, of the unsteady coexistence point) then $s_u = s^*$ – the axis is stable up to the point with the same resource concentration as the steady state.

We distinguish two regions as a function of d. For $d < 1$ (left panel), substrate consumption is not too rapid so that the producing phenotype can support a separate homogeneous population (the exclusion point). This corresponds to the light gray area $R < b + 1$, namely a selection coefficient (R) not too large relative to transitions (b). In this region the coexistence point is both unphysical and unstable. Crossing the line $R = b + 1$, one goes through a transcritical bifurcation where the two fixed points merge and exchange stability properties; in the dark gray the stable state is the coexistence fixed point. In the checkered region, the coexistence fixed point loses its stability and a stable limit cycle appears through a Hopf bifurcation.

For $d > 1$ (right panel), only coexistence states are possible, since producing cells are consuming the resource too fast to support a separate population. Once again dark gray represents the region of stable coexistence fixed points which lose the stability in the checkered region, where a stable limit cycle appears. In both sub-plots, the limit cycle (checkered) region implies sustained oscillation between producers and non-producers as a function of time. With all other parameters held fixed, this region fills more of the coexistence region as the value of $\mu'(s^*)$ decreases, but the overall coexistence area in parameter space (dark gray + checkered) does not change (see Appendix E.2).

Now we combine what we have learned about the two cases separately to understand the qualitative nature of the dynamics under environment-mediated feedback. With the Heaviside function model (12), the plane $s = s^0$ divides phase space into two regions, in each of which there are only one-sided transitions. Therefore locally the dynamics reduce to one of the two systems described above. Now the behavior of the system depends on the threshold level.

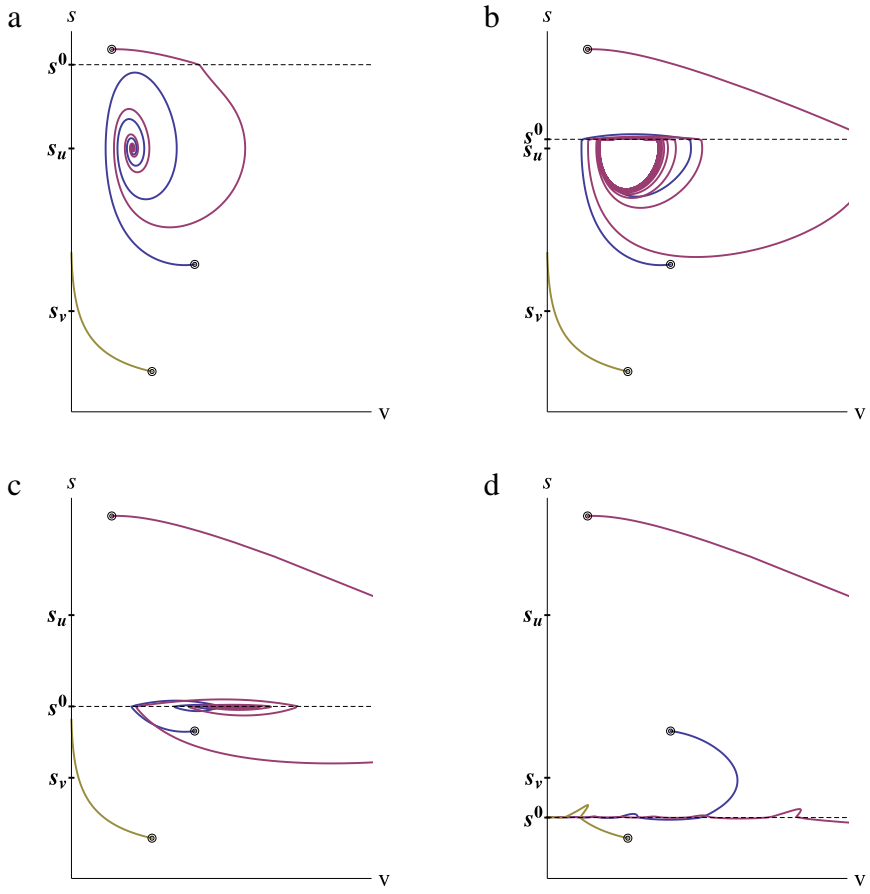

Fig. 7. Projection on the (v, s) plane of numerical trajectories of Eq. (2) with repression by the extracted substrate for different values of the threshold s^0. $b_1(s)$ and $b_2(s)$ are smoothed threshold functions (see text). The nature of the trajectories depend on the location of s^0 relative to the one-way transitions characteristic s_u and s_v (see text). When the threshold is far from the fixed point, panel (a), the trajectories are attracted to the non-trivial fixed point in the lower region. As the threshold value is lowered toward s_u, limit cycles appear on the threshold. At an even lower threshold the cycles decrease in size around the threshold. When the threshold decrease to around s_v or smaller, the trajectories are attracted by the s axis. (Parameters—$b = 0.7$, $R = 2$, $d = 0.4$, $\mu_0 = 1.5$, $k = 1$, $\lambda = 400$).

In Fig. 7 a projection of the numerically calculated trajectories on the (s, v) plane is plotted, for a soft sigmoid threshold: $b_1(s) = (1 - e^{-\lambda s})^{-1}$, $b_2(s) = 1 - b_1(s)$, where λ is the smoothness parameter. Using a softer threshold, for the purpose of numerical integration, makes the trajectories smoother and moves the fixed point slightly but does not change our analysis of the attractors.

For a trajectory that is entirely in the lower part of phase space, $s < s^0$, the dynamics will just converge to one of the three possible attractors we discussed. The fate of trajectories that start or cross over to the other region $s > s^0$ depends on the relation between the model threshold s^0 and the thresholds that emerge in the stability analysis. If $s^0 \gg s_u$ then above the threshold there are no stable states and trajectories will be attracted by the stable part of the axis below s_v, which is below s^0. Thus it will always eventually cross the threshold s^0 to lower values of s and converge to the appropriate lower part steady state. Note that for some initial conditions (small population sizes) the trajectory might encounter a stable part of the s axis below s_u and stay on this trivial fixed point (see Fig. 7(a)).

If the threshold s^0 is close to s_u, but still above s_v as in Fig. 7(b), a trajectory approaching the coexistence point, for instance, may cross the plane upward and then no longer feel the attraction of the fixed point. It then moves in the upper region towards the stable portion of the s axis, which is still below the threshold and therefore cross it once more. Then the trajectory will get caught by the spiral of the coexistence point again, which may once again take it around and make it cross the plane. This may create a stable limit cycle, especially if $s^0 < s_u$ (as in Fig. 7(c)) and the lower region fixed point becomes unattainable so the trajectory can either settle on a limit cycle or end up on a trivial fixed point on the s axis.

As the threshold is further lowered, the cycle becomes smaller and closer to the plane. Finally, when the threshold is lowered below even s_v as in Fig. 7(d), there are trivial fixed points also in the region above the threshold and the trajectories will be attracted there instead of producing the limit cycles (again, depending on initial conditions).

4. Discussion

Microorganisms address the need for actively extracting resources from their surrounding by expressing and secreting extracellular proteins which can react with the environment to produce the required resources. Because this action entails a cost in fitness, and because its products are available in the environment for neighboring cells, it can be considered a special case of the more abstract problem of cooperation. However, in contrast to the abstract setting of the problem, microorganism populations provide us the opportunity to investigate biological details of the processes that underlie this cooperative interaction.

In this work we have used nonlinear dynamical systems to describe how properties of protein expression in the single cell are reflected in the population dynamics with interactions mediated by the proteins. In particular we described two such intracellular effects. First, a random phenotypic switching between protein producing and non-producing states, such as that induced by epigenetic processes (Telomere Position Effect). Second, a regulatory process—the repression of protein expression by the produced resource, such as that seen in exoenzyme hydrolyzing complex sugars which are repressed by the resulting glucose,

or in siderophore repression by iron (Gancedo, 1998; Kummerli et al., 2009). Producing and non-producing cells interact indirectly through their common resource, in a two-way interaction: the resource both limits growth, and is being produced by one of the sub-population.

If switching rates vanish and each phenotype is completely stable, our problem is reduced to that of two competing species; in this case, in a mixed environment non-producers will always take over the population and when the resource is essential extinction will follow. When switching is driven by random epigenetic transitions, we have found a finite nonzero threshold of switching rates above which the two phenotypes can coexist in an asymptotically stable fixed point. The finding of such a threshold, regardless of the exact values of system parameters where it is found, is a qualitative prediction of the model. Genetic technology in yeast allows one to engineer strains with varying transition rates depending on the position of the gene with respect to the telomere (Louis, 1995), and thus to test this prediction experimentally.

The heterogeneous coexistence state can contribute to the fitness of a population facing the task of active resource extraction. If all cells were to produce an exoenzyme, the metabolic cost would be large; if none would produce it, the cost in terms of growth rate would be large; a static partitioning of the population into two phenotypes cannot be stable, since the non-producing cells would take over. Hence the solution of dynamic heterogeneity is a compromise between these constraints at the population level. More quantitatively, we have shown that under some conditions, there is a value of the switching rate that maximizes the population density when other system parameters are fixed. Given the variable nature of the SUC gene family expressing invertase in yeast, one can imagine a degree of freedom that is not necessarily genetic but relies on activation and silencing of different SUC genes, to tune this transition rate as required. A population which "divides labor" among producers and non-producers can have an advantage when competing with other populations in the same habitat. While this proposed role of population heterogeneity in active resource extraction is speculative, it adds to the recently accumulating evidence that such heterogeneity is advantageous at the population level under challenging conditions such as nutrient limitation at stationary phase (Veening et al., 2008a,b) or temporally varying environments (Donaldson-Matasci et al., 2008).

Our dynamic analysis enabled us to show that in some switching regimes (when the two-way transitions are approximately symmetric), the population undergoes a relaxation of its internal structure while a separate and weakly coupled external process is responsible for equilibrating the total population with its environment. This separation into two weakly coupled processes provides a simplified description of the dynamics and allows one to lower the effective dimensionality of the problem. Further investigation is required in order to characterize the generality of this decoupling in other models of populations with indirect interactions through the environment.

Under conditions of high cell density, repression by the product becomes a dominant dynamic effect. It causes an effective negative feedback on gene expression from the environment through the expression product itself. We have shown that in the presence of such repression coexistence can come about by limit-cycle dynamics, namely a stable state in which not only the individual phenotype but also the population composition cycles between different values over time. Limit-cycle dynamics between cooperators and defectors was found in Hauert et al. (2008), where an abstract public-good games was analyzed in which the effective group size for interaction induces the negative feedback; in our case it is induced by the molecular biology of gene expression mechanisms. The limit-cycle dynamics we found is analogous to predator–prey systems, however here the same population both consumes and produces the substrate needed for growth.

The modeling approach used here can be extended in several directions. First, finite-population effects can be taken into account by considering the discrete nature of cells instead of continuous population densities. In particular, extinction probabilities and other rare events that arise from this finiteness are neglected in our model. Second, the spatial structure of populations can be taken into account; the assumption of a well-mixed environment, rendering the interaction among individuals completely homogeneous, is inadequate for many biological situations. Finally, the continuous variability of gene expression in the population can be modeled, extending the binary picture of producing/non-producing cells suggested here. It is expected that the broad range of gene expression levels generally found in isogenic microorganism populations will have an important effect on the dynamics of the population when actively extracting resource (Avery, 2006; Brenner et al., 2006).

Appendix A. Active extraction of a growth-limiting source

A single phenotype which actively extracts its own growth-limiting resource from a well-mixed environment can be described by the following equations

$$\dot{\tilde{u}} = \tilde{u}(\tilde{\mu}(\tilde{s}) - D) \tag{A.1}$$

$$\dot{\tilde{s}} = \tilde{g}(\tilde{u}) - \frac{1}{Y}\tilde{\mu}(\tilde{s})\tilde{u}, \tag{A.2}$$

where $\tilde{u}$ is the population density, $\tilde{s}$ the growth-limiting resource, D the death (or washout) rate and Y the yield coefficient — the ratio of growth to amount of substrate consumed. It is characterized by two nonlinear functions, $\tilde{\mu}(\tilde{s})$ — the growth as a function of resource, and $\tilde{g}(\tilde{u})$ — the resource production as a function of cell concentration. The first is assumed monotonically increasing and saturating, such as the Monod growth function, a typical growth-rate dependence of microorganisms on a limiting resource. The second function is assumed similarly sub-linear and increasing in the concentration of cells. This describes a resource-producing reaction which is limited by the concentration of the external substrate. It is assumed that the concentration of exoenzyme is proportional to the concentration of producing cells $\tilde{u}$.

Transforming these equations to dimensionless units the death rate is equal to one ($t = D \cdot \tilde{t}$) and the maximal extraction rate is one ($\lim_{u\to\infty} g(u) = 1$). Dimensionless parameters are the maximum of the rescaled dimensionless growth function μ_0, the dimensionless inverse yield $d = Y^{-1}$, and additional parameters of the nonlinear functions $\mu(s), g(u)$ — such as the value of their argument at half maximum for the case of Monod functions. The qualitative behavior of the system is insensitive to the exact forms of both nonlinear functions and depend on their gross features: monotonicity and sublinearity. The final dimensionless equations are presented in the main text (Eq. (1)) and the detailed more general transformation is shown explicitly in the next Appendix.

The above dynamical system exhibits bifurcations as a function of the parameters μ_0 and d, allowing a nontrivial fixed point if death is not too rapid relative to maximal growth ($\mu_0 > 1$) and if resource consumption is not too rapid relative to its production at low cell concentration ($d < g'(0) = 1$). Under these conditions the fixed point obeys

$$\mu(s^*) = 1 \tag{A.3}$$
$$u^* = g(u^*)/d$$

with eigenvalues of the Jacobian at the fixed point

$$\lambda_\pm = \frac{1}{2}(-\mathrm{d}\mu'(s^*)u^* \pm \sqrt{(\mathrm{d}\mu'(s^*)u^*)^2 + 4\mu'(s^*)u^*(g'(u^*) - d)}) \tag{A.4}$$

both with negative real parts, rendering the fixed point stable for any monotonic growth function $\mu(s)$. The discriminant can be

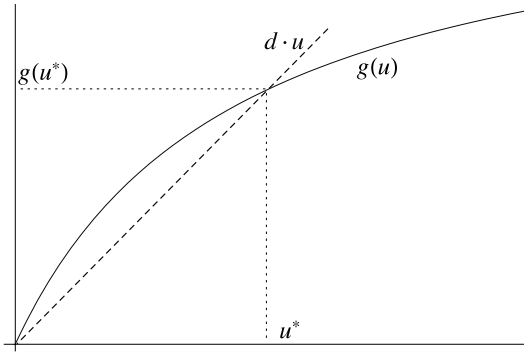

Fig. A.8. Nonlinear functions of the model for active extraction of a growth-limiting resource. The solid curve is the resource production function $g(u)$, while the dashed line is the consumption function at the fixed point. Those two curves cross at the fixed point according to (A.3), and the slope of the line will always be greater than that of the tangent to the curve at u^*.

written as follows:

$$\Delta = \mathrm{d}\mu'(s^*)u^* \left[\mathrm{d}\mu'(s^*)u^* - 4\left(1 - \frac{g'(u^*)}{d}\right)\right]. \tag{A.5}$$

While the first term in the brackets is always positive, the second is negative for any resource production function which is a rising concave function that tends to saturation. This term, representing the difference between the slopes at the fixed point of the production function g and the consumption function $\mathrm{d}\mu(s^*)u^* = \mathrm{d}u^*$, is clearly negative by (A.3) and the concaveness of $g(u)$ (see Fig. A.8). If $\frac{1}{d}(d - g'(u^*)) > \frac{1}{4}\mathrm{d}\mu'(s^*)u^*$ the discriminant is negative and there are two complex conjugate eigenvalues with a real part $-\frac{1}{2}\mathrm{d}\mu'(s^*)u^*$. Trajectories are then spirally converging with an exponent of the order of $\mathrm{d}\mu'(s^*)u^*$. If $\frac{1}{d}(d - g'(u^*)) < \frac{1}{4}\mathrm{d}\mu'(s^*)u^*$ the discriminant is positive and there are two different real eigenvalues with $0 > \lambda_2 > -\frac{1}{2}\mathrm{d}\mu'(s^*)u^* > \lambda_1 > -\mathrm{d}\mu'(s^*)u^*$, and trajectories are exponentially decaying. We conclude that in most cases the timescale of Eq. (1) will be close to $\mathrm{d}\mu'(s^*)u^*$. Only when $g'(u^*)$ is very close to d, will the decay be faster than $\mathrm{d}\mu'(s^*)u^*$.

We note that since this timescale approximation is based only a local calculation near the fixed point, domain boundary effects can modulate it. Specifically, when the trajectory approaches the s axis for small values of u there is a critical slowing down of the dynamics.

Appendix B. Simplified model equations for resource extraction by two phenotypes

Here we specify the assumptions underlying our model equations for two phenotypes, one which produces the resource by active extraction and one which does not. The equations are generally:

$$\begin{cases} \dot{\tilde{u}} = (\tilde{\mu}_u(\tilde{s}) - \tilde{D}_u)\tilde{u} - \tilde{b}_1\tilde{u} + \tilde{b}_2\tilde{v} \\ \dot{\tilde{v}} = (\tilde{\mu}_v(\tilde{s}) - \tilde{D}_v)\tilde{v} + \tilde{b}_1\tilde{u} - \tilde{b}_2\tilde{v} \\ \dot{\tilde{s}} = \tilde{c}\dfrac{\tilde{u}}{\tilde{u}+\tilde{z}} - \dfrac{1}{\tilde{Y}_u}\tilde{\mu}_u(\tilde{s})\tilde{u} - \dfrac{1}{\tilde{Y}_v}\tilde{\mu}_v(\tilde{s})\tilde{v} \end{cases} \tag{B.1}$$

where $\tilde{u}$, $\tilde{v}$ are concentrations of the producing and non-producing phenotype populations respectively, $\tilde{s}$ is the limiting resource concentration, $\tilde{\mu}_i(s)$ the specific growth rates, $\tilde{D}$ the removal rate due to death or washout, $\tilde{b}_i$ the transition rates between the phenotypes (which can generally be dependent on $\tilde{s}$), $\tilde{c}$ and $\tilde{z}$ constants of the resource production function and $\tilde{d}_i = \tilde{Y}_u^{-1}$ the inverse of the yield for the two phenotypes.

In the mathematical analysis of the model no specific form for the growth function $\tilde{\mu}(\tilde{s})$ was assumed; it was required only that it is monotonically increasing and vanishing for $\tilde{s} = 0$. This last assumption is based on the extreme situation where the only source of growth for the cells is the resource produced by the cells. This can be unrealistic in many situations, including the invertase case since the cells have a limited ability to absorb sucrose directly and express also a form of intracellular invertase. Relaxing the mathematical assumption $\tilde{\mu}(0) = 0$ leads to complications in the model analysis and does not allow many of the approximations presented in the text. However, we solved the equations numerically with a constant baseline production term for both phenotypes, and observed that the qualitative results presented in the main text, such as the threshold on the transition rates, the decoupling of internal and external dynamics, and the limit cycle for the repression regime—all remain as empirically observed phenomena. Wherever numerical integration was performed for visualization, a Monod growth function of the form $\tilde{\mu}(s) = \tilde{\mu}_0 \frac{\tilde{s}}{\tilde{k}+\tilde{s}}$ was used.

We assumed that the different phenotypes display the same form of the growth function, only scaled by a selection coefficient R: $\tilde{\mu}_v(\tilde{s}) = R\tilde{\mu}_u(\tilde{s}) = R\tilde{\mu}(\tilde{s})$, where $R > 1$ representing the metabolic cost of the exoenzyme production. We further assume that while the different phenotypes have different growth rates and different yields, their substrate consumption rate is identical, and define a new global consumption rate parameter $\tilde{d} := \tilde{d}_u = \tilde{d}_u$. Finally, we assume that removal occurs at the same rate, $\tilde{D} := \tilde{D}_u = \tilde{D}_v$. Now we can rescale time accordingly so the removal rates are 1. By rescaling $\tilde{u}$ and $\tilde{s}$ we can set both $\tilde{c}$ and $\tilde{z}$ to be also 1. We shall also rescale $\tilde{v}$ similarly to $\tilde{u}$ so the first two equations remain symmetric. By redefining all the other dimensionless constants, we arrive at the a simplified and dimensionless form for the equations, Eq. (2) in the main text. The overall transformations of all variables and parameters to dimensionless quantities are:

$$t = \tilde{D}\cdot\tilde{t} \qquad b = \frac{1}{\tilde{D}}\cdot\tilde{b}$$

$$u = \frac{1}{\tilde{z}}\cdot\tilde{u} \qquad d = \frac{\tilde{D}\tilde{z}}{\tilde{c}}\cdot\tilde{d}$$

$$v = \frac{1}{\tilde{z}}\cdot\tilde{v} \qquad \mu(s) = \frac{1}{\tilde{D}}\cdot\tilde{\mu}(\tilde{s}) = \frac{\mu_0 s}{s+k}$$

$$s = \frac{\tilde{D}}{\tilde{c}}\cdot\tilde{s} \qquad \mu_0 = \frac{1}{\tilde{D}}\cdot\tilde{\mu}_0$$

$$k = \frac{\tilde{D}}{\tilde{c}}\tilde{k}.$$

In the main text and in the following only the dimensionless quantities appear.

Appendix C. Fixed points and stability for random switching

The fixed points of the dynamical system with constant b's are found by the equations:

$$(\mu(s^*) - 1)u^* + bv^* - bu^* = 0 \tag{C.1}$$

$$(R\mu(s^*) - 1)v^* - bv^* + bu^* = 0 \tag{C.2}$$

$$\frac{u^*}{u^*+1} - d(u^*+v^*)\mu(s^*) = 0. \tag{C.3}$$

These equations have the trivial solution, $u^* = v^* = 0$, for any value of s; this means that the entire s axis is a continuum of fixed points (see below). We now wish to find the nontrivial states. By summing Eqs. (C.1) and (C.2)

$$\frac{u^*}{v^*} = -\frac{R\mu(s^*) - 1}{\mu(s^*) - 1}. \tag{C.4}$$

In order for this ratio to be positive, $R^{-1} < \mu(s^*) < 1$. By substituting (C.4) into (C.2) we get a quadratic equation for $\mu(s^*)$

$$d < \frac{1+R}{4}. \tag{C.8}$$

$$b > B(R,d) := \frac{R^2 + 4d^2(R-1) - d(R(R+3)-2) + (d+(d-1)R)\sqrt{R^2 - 4d(R-1)}}{2d(R-1)(1-4d+R)}. \tag{C.9}$$

Box I.

with one valid solution:[1]

$$\mu(s^*) = \frac{(1+R)(1+b) - \sqrt{(1+R)^2(1+b)^2 - 4R(1+2b)}}{2R}. \tag{C.5}$$

The ratio Eq. (C.4) is independent of the dynamics of the environment (Eq. (C.3)). Using (C.4) and (C.3), we find for each sub-population:

$$u^* = \frac{R\mu(s^*) - 1 - d(R-1)\mu(s^*)^2}{d(R-1)\mu(s^*)^2} \tag{C.6}$$

$$v^* = \frac{1-\mu(s^*)}{R\mu(s^*)-1}\frac{R\mu(s^*) - 1 - d(R-1)\mu(s^*)^2}{d(R-1)\mu(s^*)^2}. \tag{C.7}$$

The condition for coexistence (demanding nonzero u^* from (C.6)) can be formulated as two inequalities, as explained qualitatively in the text: Eqs. (C.8) and (C.9) are given in Box I.

C.1. Stability of the trivial solution

The stability of the trivial solution on the s axis is determined by the Jacobian on the axis:

$$J = \begin{pmatrix} \mu(s) - 1 - b & b & 0 \\ b & R\mu(s) - 1 - b & 0 \\ 1 - \mathrm{d}\mu(s) & -\mathrm{d}\mu(s) & 0 \end{pmatrix}. \tag{C.10}$$

With eigenvalues

$$\lambda_\pm = -1 - b + \frac{1+R}{2}\mu(s) \pm \sqrt{b^2 + \left(\frac{1-R}{2}\right)^2 \mu^2(s)} \tag{C.11}$$

$$\lambda_0 = 0. \tag{C.12}$$

One of the eigenvalues (λ_0) is always zero, with a corresponding eigenvector tangent to the s axis. By the Center Manifold Theorem (Guckenheimer and Holmes, 1990), each point on the axis has a one dimensional center manifold, the s-axis itself. Since the flow is constant along the axis, the solution on the center manifold is stable (although not asymptotically stable). To prove stability it is therefore enough to prove that there is no unstable manifold, or that the sign of the other two eigenvalues is negative.

At $s = 0$ both other eigenvalues (λ_+, λ_-) are negative, so it is always stable. At positive values of s, since $\lambda_+ > \lambda_-$ it is enough to require $\lambda_+ < 0$ to ensure stability. Since $\mu(s)$ in monotonic, $\lambda_+(s)$ is also an increasing function of s, and the axis is stable from the origin up to the point where $\lambda_+(s) = 0$. Solving this condition for $\mu(s)$ we arrive at (C.5), our previous expression for s^*—the value of the coexistence point s component; therefore the s axis is stable only for $s < s^*$. For larger s, the s-axis becomes unstable and trajectories move away from it towards the coexistence point (if it exists) or towards a lower, stable point on the axis itself, below s^*.

C.2. Stability of the coexistence solution

In this section we prove the stability of the coexistence solution by using the Routh–Hurwitz conditions to show that all the eigenvalues have negative real parts. For a three dimensional system, these conditions are:

$$a_0 a_1 > 0 \tag{C.13}$$

$$a_1 a_2 - a_0 a_3 > 0 \tag{C.14}$$

where a_i's are coefficients of the characteristic polynomial: $a_0\lambda^3 + a_1\lambda^2 + a_2\lambda + a_3 = 0$.

Since at the coexistence fixed point the following relations hold

$$\mu(s^*)(u^* + Rv^*) = u^* + v^* \tag{C.15}$$

$$-b\frac{v^*}{u^*} = \mu(s^*) - 1 - b \tag{C.16}$$

$$-b\frac{u^*}{v^*} = R\mu(s^*) - 1 - b. \tag{C.17}$$

The Jacobian there takes the form (dropping the asterisk from now on):

$$J = \begin{pmatrix} -b\frac{v}{u} & b & \mu'(s)u \\ b & -b\frac{u}{v} & R\mu'(s)v \\ \frac{1}{(1+u)^2} - \mathrm{d}\mu(s) & -\mathrm{d}\mu(s) & -d(u+v)\mu'(s) \end{pmatrix}. \tag{C.18}$$

Then, the coefficients of the characteristic polynomial for the coexistence point are:

$$\begin{aligned} a_0 &= -1 < 0 \\ a_1 &= \mathrm{tr}J = -b\left(\frac{u}{v} + \frac{v}{u}\right) - d(u+v)\mu' < 0 \\ a_2 &= -b\mathrm{d}\mu'(u+v)\left(\frac{u}{v} + \frac{v}{u}\right) - \mathrm{d}\mu\mu'(Rv+u) + \mu'\frac{u}{(1+u)^2} \\ a_3 &= -b\mathrm{d}\mu\mu'\left(u + R\frac{v}{u}v + Rv + \frac{u}{v}u\right) \\ &\quad + b\mu'\left(Rv + \frac{u}{v}u\right)\frac{1}{(1+u)^2}. \end{aligned}$$

The first Routh–Hurwitz condition (C.13) is clearly valid. As for the second one, using (C.3):

$$\begin{aligned} \frac{a_1a_2 - a_0a_3}{\mathrm{d}\mu'} &= \mathrm{d}\mu'(u+v)^2\left[b\left(\frac{u}{v} + \frac{v}{u}\right) + 1 - \mathrm{d}\mu^2\left(1 + \frac{v}{u}\right)\right] \\ &\quad + bv\Bigg[b\left(\frac{u}{v} + 1\right)\left(\frac{u}{v} + \frac{v}{u}\right)^2 + \mathrm{d}\mu^2(R-1) \\ &\quad \times \left(1 + \frac{v}{u}\right)^2 + \mu\left(\frac{u}{v} - 1\right)(R-1)\Bigg]. \end{aligned} \tag{C.19}$$

Since the factors preceding the brackets are all positive, for the second condition (C.14) to be valid it is enough to prove that each of the expressions in the brackets is positive. For the first bracket one can write the following bound:

$$\begin{aligned} b\left(\frac{u}{v} + \frac{v}{u}\right) + 1 - \mathrm{d}\mu^2\left(1 + \frac{v}{u}\right) &> b\frac{v}{u} + 1 - \mathrm{d}\mu^2\left(1 + \frac{v}{u}\right) \\ &= 2 - \mu + b - \mu\frac{\mathrm{d}\mu^2(R-1)}{R\mu - 1} \end{aligned}$$

[1] The other solution will result in a negative steady state ratio between the two sub-populations.

where we used the fixed point conditions (C.16) and (C.17). Using the positivity of the steady state value of u (C.6):

$$2-\mu+b-\mu\frac{\mathrm{d}\mu^2(R-1)}{R\mu-1} > 2-\mu+b-\mu\cdot 1 = 2(1-\mu)+b.$$

Since the value of the growth function at the fixed point is always smaller than 1, this last expression is indeed positive. For the second bracket in Eq. (C.19):

$$\begin{aligned} &b\left(\frac{u}{v}+1\right)\left(\frac{u}{v}+\frac{v}{u}\right)^2+\mathrm{d}\mu^2(R-1)\left(1+\frac{v}{u}\right)^2 \\ &\quad+\mu\left(\frac{u}{v}-1\right)(R-1) \\ &> b\left(\frac{u}{v}+1\right)\left(\frac{v}{u}\right)^2+\mu(-1)(R-1) \\ &= \mu\frac{R-1}{R\mu-1}[2+b-\mu(1+R)], \end{aligned}$$

where we have used (C.4), (C.16) and (C.17) again. In the last expression everything outside of the brackets is positive. The expression inside the brackets can be shown to be positive using the value of the growth function at steady state (C.5) and elementary algebra.

Appendix D. Decoupling approximation

As stated in the main text, the decoupling phenomenon appears for different parameter values. It can be developed as a controlled approximation using singular perturbation theory (O'Malley, 1974) in the limit of very large b, or small $\epsilon = 1/b \ll 1$. Then the equations are

$$\begin{aligned} \dot{w} &= w\left(\frac{r+R}{r+1}\mu(s)-1\right) \\ \epsilon\dot{r} &= -\epsilon\mu(s)(R-1)r-(r^2-1) \\ \dot{s} &= \frac{w}{w+1+1/r}-\mathrm{d}\mu(s)w. \end{aligned} \tag{D.1}$$

The solution can be expanded in powers of ϵ as long as we allow different behaviors in a boundary layer about the size of ϵ. Defining a fast time scale $\tau = t/\epsilon$, the first order expansion will be:

$$\begin{aligned} w(t,\tau,\epsilon) &= w_0^t(t)+\epsilon w_1^t(t)+\epsilon w_1^\tau(\tau)+\cdots \\ s(t,\tau,\epsilon) &= s_0^t(t)+\epsilon s_1^t(t)+\epsilon s_1^\tau(\tau)+\cdots \\ r(t,\tau,\epsilon) &= r_0^t(t)+r_0^\tau(\tau)+\epsilon r_1^t(t)+\epsilon r_1^\tau(\tau)+\cdots. \end{aligned}$$

Notice that the fast part of the solution for r is the only one which has a zero order term since the equation for $\dot{r}$ depends on ϵ explicitly. The fast part of the solution (that depends on τ) must tend to zero as τ tends to infinity, and the slow part (that depends only on t) must solve the equations by itself, albeit with a different initial condition. The slow solution can be obtained iteratively by algebraically finding the value of the current order of $r(t)$ and then solving two differential equations for $w(t)$ and $s(t)$. In the first iteration (terms of ϵ^0):

$$\begin{aligned} 0 &= -((r_0^t(t))^2-1) \\ r_0^t(t) &= 1 \end{aligned}$$

$w_0(t)$ and $s_0(t)$ can then be found from:

$$\begin{aligned} \dot{w}_0^t &= w_0^t\left(\frac{1+R}{2}\mu(s_0^t)-1\right) \\ \dot{s}_0^t &= \frac{w_0^t}{w_0^t+2}-\mathrm{d}\mu(s_0^t)w_0^t. \end{aligned}$$

The dynamics of the total population and the substrate determine the slow time scale.

Now, by using the form of the slow solution, we can find new equations for the fast solution. Again taking zero order (ϵ^0) in r:

$$\begin{aligned} \partial_\tau r_0^\tau(\tau) &= -((r_0^\tau(\tau)+r_0^t(t))^2-1) \\ \partial_\tau r_0^\tau(\tau) &= -(r_0^t(t))^2-2r_0^\tau(\tau)r_0^t(t)-(r_0^\tau(\tau))^2+1. \end{aligned}$$

Using the slow solution $r_0^t(t) = 1$:

$$\partial_\tau r_0^\tau(\tau) = -2r_0^\tau(\tau)-(r_0^\tau(\tau))^2.$$

Solving:

$$r_0^\tau(\tau) = \frac{2A}{\mathrm{e}^{2\tau}-A}.$$

With A determined by the initial conditions. The full solution in this order is

$$r_0(t) = r_0^t(t)+r_0^\tau(bt) = \frac{\mathrm{e}^{2bt}+A}{\mathrm{e}^{2bt}-A} = \tanh(bt+C). \tag{D.2}$$

Only in the next order will corrections to s and w appear.

It will be shown now that assuming decoupling in the general case, the ratio behaves as a hyperbolic tangent. This is not a controlled approximation but shows the generality of the above result. The equation for the ratio r when $\mu(s)$ is assumed constant is

$$\dot{r} = -ar-b(r^2-1)$$

with $a = \mu(s)(R-1)$.

Integrating by separation of variables:

$$\int \mathrm{d}t = \int \frac{\mathrm{d}r}{-ar-b(r^2-1)}.$$

Integrating, the RHS integral depends on the values of r in the integration:

$$t+C = \begin{cases} \dfrac{2}{\sqrt{a^2+4b^2}}\operatorname{atanh}\left(\dfrac{a+2br}{\sqrt{a^2+4b^2}}\right) \\ \quad a+2br < \sqrt{a^2+4b^2} \\ \dfrac{2}{\sqrt{a^2+4b^2}}\operatorname{acoth}\left(\dfrac{a+2br}{\sqrt{a^2+4b^2}}\right) \\ \quad a+2br > \sqrt{a^2+4b^2}. \end{cases}$$

Denoting either tanh or coth by T we can solve for $r(t)$:

$$r(t) = -\frac{a}{2b}+\frac{\sqrt{a^2+4b^2}}{2b}\mathrm{T}\left[\frac{\sqrt{a^2+4b^2}}{2}(t+C)\right].$$

With C and T determined by initial conditions. Returning to the original parameters and writing the cases explicitly:

$$r(t) = -\frac{\mu(s)(R-1)}{2b}+\frac{\sqrt{(\mu(s)(R-1))^2+4b^2}}{2b} \tanh\left[\frac{\sqrt{(\mu(s)(R-1))^2+4b^2}}{2}(t+C)\right].$$

If

$$r(0) < -\frac{\mu(s)(R-1)}{2b}+\frac{\sqrt{(\mu(s)(R-1))^2+4b^2}}{2b}.$$

Or

$$r(t) = -\frac{\mu(s)(R-1)}{2b}+\frac{\sqrt{(\mu(s)(R-1))^2+4b^2}}{2b} \coth\left[\frac{\sqrt{(\mu(s)(R-1))^2+4b^2}}{2}(t+C)\right].$$

If

$$r(0) > -\frac{\mu(s)(R-1)}{2b} + \frac{\sqrt{(\mu(s)(R-1))^2+4b^2}}{2b}.$$

The solution always stays on the same side of the line $r^* \equiv r(\infty) = -\frac{\mu(s)(R-1)}{2b} + \frac{\sqrt{(\mu(s)(R-1))^2+4b^2}}{2b}$. From the form of the solution it is evident that the characteristic timescale is of the order $(4b^2+(R-1)^2\mu(\bar{s})^2)^{-\frac{1}{2}}$, as was presented in (9). The perturbation theory approximation (D.2) is a specific well-controlled case of this general solution.

Appendix E. Analysis of the single-sided transition models

In this Appendix we analyze the two one-sided transitions cases that make up the model Eq. (2) with the transition rates defined by Eq. (12). We detail the steady states and dynamics of each one-sided problem that were combined in the main text in the treatment of this model.

E.1. Transitions to non-producing state

Since the resource is essential for growth, only trivial fixed points are found in this case, with arbitrary values of s. The stability of points on the s-axis depends on the value of s and is determined by the Jacobian:

$$J = \begin{pmatrix} \mu(s)-1-b & 0 & 0 \\ b & R\mu(s)-1 & 0 \\ -\mathrm{d}\mu(s) & -\mathrm{d}\mu(s) & 0 \end{pmatrix}. \tag{E.1}$$

With the eigenvalues:

$$\begin{aligned} \lambda_1 &= \mu(s)-1-b \\ \lambda_2 &= R\mu(s)-1 \\ \lambda_3 &= 0. \end{aligned} \tag{E.2}$$

It is seen that $R\mu(s) < 1$ is a sufficient condition for stability and so $s_v = \mu^{-1}(1/R)$ is the point where the axis loses stability. Generally, trajectories will curve around, repelled from the unstable part of the axis and attracted to the stable part. Numerical solutions verify this for various parameter values (see Fig. E.9). In all cases, eventually, the population will consist almost entirely of non-producing cells and v and s will decrease monotonically until there are no more cells.

E.2. Transitions to producing state

In this case also, there are trivial fixed points on the axis up to a certain s value. Again examining the Jacobian on the axis:

$$J = \begin{pmatrix} \mu(s)-1 & b & 0 \\ 0 & R\mu(s)-1-b & 0 \\ -\mathrm{d}\mu(s) & -\mathrm{d}\mu(s) & 0 \end{pmatrix}. \tag{E.3}$$

We now have eigenvalues:

$$\begin{aligned} \lambda_1 &= \mu(s)-1 \\ \lambda_2 &= R\mu(s)-1-b \\ \lambda_3 &= 0. \end{aligned} \tag{E.4}$$

So that the axis is stable up to $s_u = \min\left(\mu^{-1}(1), \mu^{-1}\left(\frac{1+b}{R}\right)\right)$. Notice that since $\mu(s)$ is increasing, $s_u > s_v$.

Unlike the previous case, however, now there are always producing cells that allow for nontrivial states with nonzero population. One finds two types of nontrivial fixed points: first, an exclusion state

$$\begin{cases} u^* = \dfrac{1}{d} - 1 \\ v^* = 0 \\ \mu(s^*) = 1 \end{cases} \tag{E.5}$$

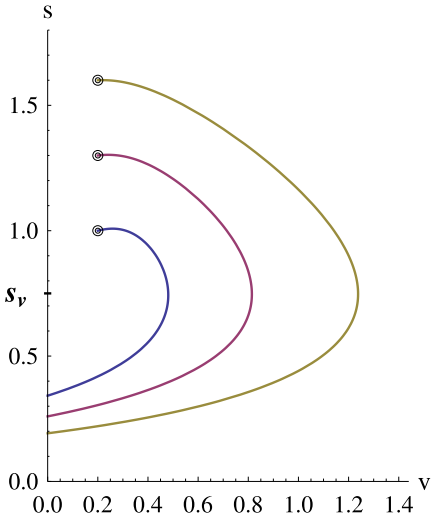

Fig. E.9. Projection on the (v, s) plane of numerical trajectories of the model in Eq. (2) with one-way transitions to the non-producing state for several different initial conditions. The extreme value in which the s-axis is stable is marked with s_v. The trajectories can be seen repelled from the part of the s-axis above s_v, and attracted to a point below it. ($b_1 = 0$, $b_2 = 1.75$, $R = 3$, $d = 0.3$, $\mu_0 = 1.8$, $K = 3$).

which requires $d < 1$, namely not too rapid a consumption. Second, a coexistence,

$$\begin{cases} u^* = \dfrac{bR^2 - d(R-1)(b+1)^2}{d(R-1)(b+1)^2} \\ v^* = \dfrac{R-b-1}{Rb} \cdot \dfrac{bR^2 - d(R-1)(b+1)^2}{d(R-1)(b+1)^2} \\ \mu(s^*) = \dfrac{b+1}{R}. \end{cases} \tag{E.6}$$

Taking on physical meaning (positive concentrations) when the following conditions are fulfilled:

$$\begin{cases} d < \dfrac{bR^2}{(R-1)(b+1)^2} \\ R > b+1. \end{cases} \tag{E.7}$$

The stability of the exclusion fixed point ($v^* = 0$) is determined by the following Jacobian

$$J = \begin{pmatrix} \mu(s^*)-1 & b & \mu'(s^*)u^* \\ 0 & R\mu(s^*)-1-b & 0 \\ \dfrac{1}{(1+u^*)^2} - \mathrm{d}\mu(s^*) & -\mathrm{d}\mu(s^*) & -\mathrm{d}\mu'(s^*)u^* \end{pmatrix}. \tag{E.8}$$

And the eigenvalues are

$$\lambda_{1,2} = \frac{1}{2}(d-1)\sqrt{\mu'(s^*)}\left(\sqrt{\mu'(s^*)} \pm \sqrt{4-\mu'(s^*)}\right) \tag{E.9}$$

$$\lambda_3 = R-b-1. \tag{E.10}$$

The first two eigenvalues always have a negative real part (recall this state exists only for $d < 1$). The third eigenvalue is negative when $R < b+1$, namely in the region where it is the only fixed point (since the coexistence point is unphysical by the second condition in (E.7)). The appearance of the coexistence fixed point at physical concentration values renders the exclusion fixed point unstable. Thus one concludes that for $d < 1$ and $R < b+1$ the exclusion point is the only nontrivial stable fixed point.

The conditions in Eq. (E.7) and numerical calculation of the eigenvalues allow us to plot the stability regions for the coexistence fixed point. Typical results for the stability regions

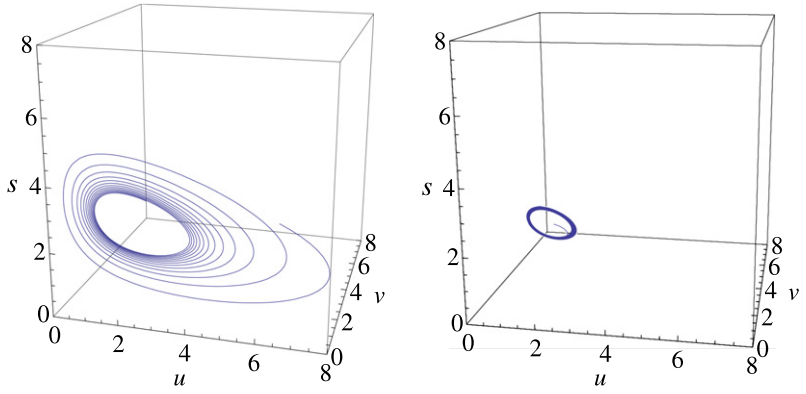

(a) Initial conditions outside the limit cycle. (b) Initial condition within the limit cycle.

Fig. E.10. Numerical trajectories of the model in Eq. (2) with one-way transitions to the producing state, demonstrating the possibility of stable limit cycles. ($b_1 = 0$, $b_2 = 1.75$, $R = 3$, $d = 0.3$, $\mu_0 = 1.8$, $K = 3$).

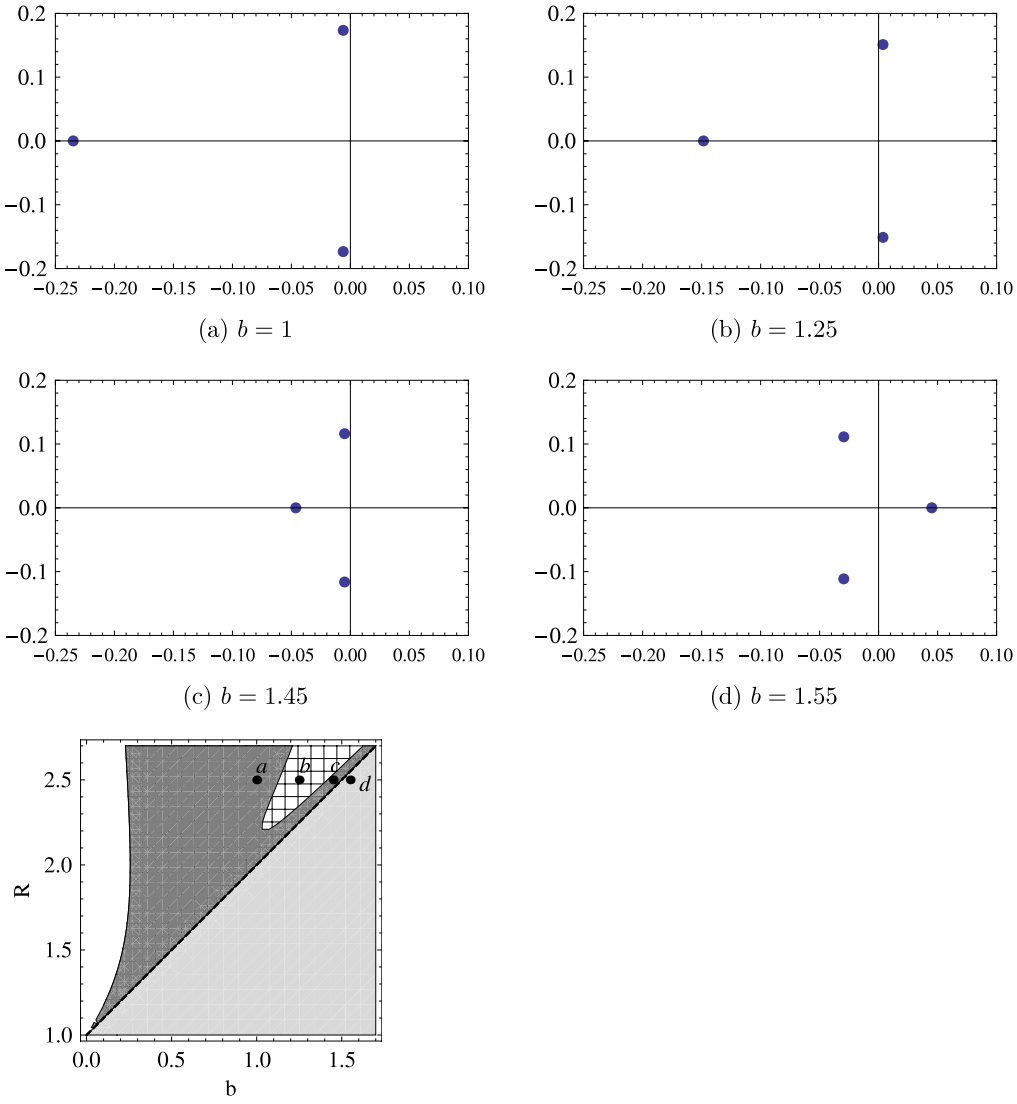

Fig. E.11. The eigenvalues of (E.11) at the coexistence point for $d = 0.65$, $\mu'(s^*) = 0.1$, $R = 2.5$. In the first four panels the eigenvalues are marked on the complex plane for four different points in parameter space corresponding to increasing values of b. In (a) all three points are on the left side of the complex plane, meaning a stable point. In (b) the two complex-conjugate eigenvalues have crossed the imaginary axis to the right side of the plane in a Hopf bifurcation and a limit cycle had appeared. At point (c) the two eigenvalues have crossed back to the left in another Hopf bifurcation and now the fixed point is stable again. Finally, in (d) the third real eigenvalue that had been steadily increasing has crossed the imaginary line and the coexistence point becomes unstable. The coexistence fixed point has gone through a transcritical bifurcation and is no longer physical.

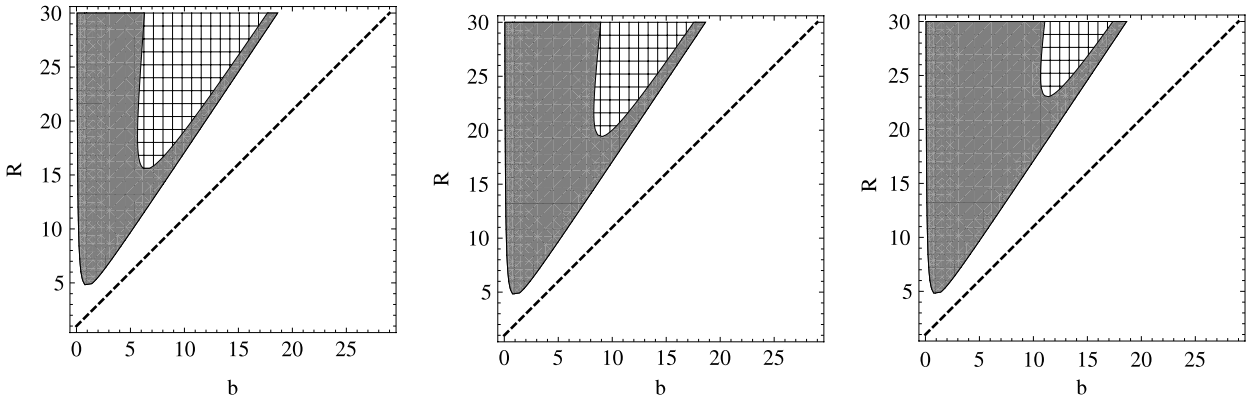

(a) $\mu'(s^*) = 0.5$. (b) $\mu'(s^*) = 1$. (c) $\mu'(s^*) = 1.5$.

Fig. E.12. Stability regions on the $b - R$ parameter space for $d = 1.5$ and different values of $\mu'(s^*)$. Shading is as in Fig. 6.

on the $b - R$ plane are displayed in Fig. 6, and two features are apparent.

First, close to the boundary of the existence region defined by Eq. (E.7) the point is stable. For $d > 1$ the boundary is defined by $bR^2 = d(R-1)(b+1)^2$, with $R \sim d/b$ for small b and $R \sim \mathrm{d}b$ for large b. By passing this curve the coexistence point becomes unphysical (negative values). For $d < 1$ part of the boundary is now defined by $R = b + 1$ and when this line is crossed, only the v^* of the coexistence point becomes negative, thus defining the exclusion state. This is a transcritical bifurcation as evident by the change of stability between the two fixed points over this line. The other part of the boundary of the dark gray region (close to the $b = 0$ axis), is determined by the other existence condition for this state (see Eq. (E.7)). Notice that since the continuum of trivial fixed points on the s axis extends up to $s_u = \min\left(\mu^{-1}(1), \mu^{-1}\left(\frac{1+b}{R}\right)\right)$, then $s_u = \mu^{-1}(1)$ if the stable state is the exclusion state and $s_u = \mu^{-1}\left(\frac{1+b}{R}\right)$ and in both cases $s_u = s^*$ (by Eqs. (E.5) and (E.6)).

Second, the stability regions clearly show a certain "cut-out" area where the coexistence point loses stability while still maintaining positive concentrations. Numerical integration shows that in this region a stable limit cycle appears around the fixed point (see Fig. E.10). This suggests a supercritical[2] Hopf bifurcation. This can be validated by looking again at the eigenvalues of the Jacobian:

$$J = \begin{pmatrix} \mu(s^*) - 1 & b & \mu'(s^*)u^* \\ 0 & R\mu(s^*) - 1 - b & R\mu'(s^*)v^* \\ \dfrac{1}{(1+u)^2} - \mathrm{d}\mu(s^*) & -\mathrm{d}\mu(s^*) & -\mathrm{d}\mu'(s^*)(u^* + v^*) \end{pmatrix}. \tag{E.11}$$

According to the Vieta formulas, the product of all three eigenvalues is the negative of the coefficient of the quadratic term in the normal form of the characteristic polynomial. That is

$$\lambda_1\lambda_2\lambda_3 = (1 + b - R)\left(\frac{(1+b)^2 d(R-1) - bR^2}{bR^2}\right)^2 \mu'(s^*). \tag{E.12}$$

Since $\mu(s)$ is monotonically increasing and $R > b + 1$ for the coexistence point to be physical, this product is always negative. This means that the only way a stable point, with the real values of all the roots negative, can become unstable continuously is when two complex conjugate roots pass through the imaginary axis, and this is the condition for a Hopf bifurcation (see Fig. E.11). On the stable side of the bifurcation, the coexistence point is a stable focus with decaying oscillations. When b is increased, the spiral no longer reaches the coexistence point but remains in a stable orbit around it. If b is further increased, this stable limit cycle will shrink back into the point in another Hopf bifurcation. Thus, in the region this stable limit cycle exists, it is the only stable attractor for the dynamics.

The shape of the limit-cycle region depends on the derivative of the growth function at the fixed point ($\mu'(s^*)$), and this is the only effect this parameter has on the stability properties of the system. As can be seen in Fig. E.12, when the value of the derivative increases, the area in parameter space where the limit cycle is stable shrinks; when it approaches zero, it tends to fill all of the area in which coexistence is possible.

[2] Since a small limit cycle always appears around the point at the bifurcation.

References

Acar, M., Mettetal, J.T., van Oudenaarden, A., 2008. Stochastic switching as a survival strategy in fluctuating environments. Nat. Genet. 40, 471–475.

Avery, S.V., 2006. Microbial cell individuality and the underlying sources of heterogeneity. Nat. Rev. Microbiol. 4, 577–587.

Balaban, N.Q., Merrin, J., Chait, R., Kowalik, L., Leibler, S., 2004. Bacterial persistence as a phenotypic switch. Science 305, 1622–1625.

Brenner, N., Farkash, K., Braun, E., 2006. Dynamics of protein distributions in cell populations. Phys. Biol. 3, 172–182.

Carlson, M., Botstein, D., 1982. Two differentially regulated mRNAs with different 5' ends encode secreted with intracellular forms of yeast invertase. Cell 28, 145–154.

Carlson, M., Botstein, D., 1983. Organization of the SUC gene family in Saccharomyces. Mol. Cell. Biol. 3, 351–359.

Chuang, J.S., Rivoire, O., Leibler, S., 2010. Cooperation and Hamilton's rule in a simple synthetic microbial system. Mol. Syst. Biol. 6, 398.

Crespi, B.J., 2001. The evolution of social behavior in microorganisms. Trends Ecol. Evol. 16, 178–183.

Diggle, S.P., Griffin, A.S., Campbell, G.S., West, S.A., 2007. Cooperation and conflict in quorum-sensing bacterial populations. Nature 450, 411–414.

Donaldson-Matasci, M., Lachmann, M., Bergstrom, C., 2008. Phenotypic diversity as an adaptation to environmental uncertainty. Evol. Ecol. Res. 10, 493–515.

Filiba, E., Lewin, D., Brenner, N., Transients and tradeoffs: heterogeneous populations in a competitive changing environment.

Gancedo, J.M., 1998. Yeast carbon catabolite repression. Microbiol. Mol. Biol. Rev. 62, 334–361.

Gore, J., Youk, H., van Oudenaarden, A., 2009. Snowdrift game dynamics and facultative cheating in yeast. Nature 459, 253–256.

Gottschling, D.E., Aparicio, O.M., Billington, B.L., Zakian, V.A., 1990. Position effect at S. cerevisiae telomeres: reversible repression of Pol II transcription. Cell 63, 751–762.

Greig, D., Travisano, M., 2004. The Prisoner's Dilemma and polymorphism in yeast SUC genes. Proc. R. Soc. Lond. B Biol. Sci. 271 (suppl. 3), S25–S26.

Griffin, A.S., West, S.A., Buckling, A., 2004. Cooperation and competition in pathogenic bacteria. Nature 430, 1024–1027.

Guckenheimer, J., Holmes, P., 1990. Nonlinear Oscillations, Dynamical Systems, and Bifurcations of Vector Fields. Springer.

Hauert, C., Holmes, M., Doebeli, M., 2006. Evolutionary games and population dynamics: maintenance of cooperation in public goods games. Proc. R. Soc. Lond. B Biol. Sci. 273, 2565–2570.

Hauert, C., Wakano, J.Y., Doebeli, M., 2008. Ecological public goods games: cooperation and bifurcation. Theor. Popul. Biol. 73, 257–263.

Jiricny, N., Diggle, S.P., West, S.A., Evans, B.A., Ballantyne, G., Ross-Gillespie, A., Griffin, A.S., 2010. Fitness correlates with the extent of cheating in a bacterium. J. Evol. Biol. 23, 738–747.
Kreft, J., 2005. Conflicts of interest in biofilms. Biofilms 1, 265–276.
Kummerli, R., Jiricny, N., Clarke, L.S., West, S.A., Griffin, A.S., 2009. Phenotypic plasticity of a cooperative behaviour in bacteria. J. Evol. Biol. 22, 589–598.
Kussell, E., Kishony, R., Balaban, N.Q., Leibler, S., 2005. Bacterial persistence: a model of survival in changing environments. Genetics 169, 1807–1814.
Kussell, E., Leibler, S., 2005. Phenotypic diversity, population growth, and information in fluctuating environments. Science 309, 2075–2078.
Lachmann, M., Jablonka, E., 1996. The inheritance of phenotypes: an adaptation to fluctuating environments. J. Theor. Biol. 181, 1–9.
Louis, E.J., 1995. The chromosome ends of *Saccharomyces cerevisiae*. Yeast 11, 1553–1573.
MacLean, R.C., 2008. The tragedy of the commons in microbial populations: insights from theoretical, comparative and experimental studies. Heredity 100, 471–477.
MacLean, R.C., Brandon, C., 2008. Stable public goods cooperation and dynamic social interactions in yeast. J. Evol. Biol. 21, 1836–1843.
MacLean, R.C., Gudelj, I., 2006. Resource competition and social conflict in experimental populations of yeast. Nature 441, 498–501.
Modak, T., Pradhan, S., Watve, M., 2007. Sociobiology of biodegradation and the role of predatory protozoa in biodegrading communities. J. Bioscience 32, 775–780.
O'Malley, R., 1974. Introduction to Singular Perturbations. In: Applied Mathematics and Mechanics, vol. 14. Academic Press.
Parsek, M.R., Greenberg, E.P., 2005. Sociomicrobiology: the connections between quorum sensing and biofilms. Trends Microbiol. 13, 27–33.
Pfeiffer, T., Schuster, S., Bonhoeffer, S., 2001. Cooperation and competition in the evolution of ATP-producing pathways. Science 292, 504–507.
Ross-Gillespie, A., Gardner, A., Buckling, A., West, S.A., Griffin, A.S., 2009. Density dependence and cooperation: theory and a test with bacteria. Evolution 63, 2315–2325.
Ross-Gillespie, A., Gardner, A., West, S.A., Griffin, A.S., 2007. Frequency dependence and cooperation: theory and a test with bacteria. Am. Nat. 170, 331–342.
Schuster, S., Kreft, J.U., Brenner, N., Wessely, F., Theissen, G., Ruppin, E., Schroeter, A., 2010. Cooperation and cheating in microbial exoenzyme production–theoretical analysis for biotechnological applications. Biotechnol. J. 5, 751–758.
Thattai, M., van Oudenaarden, A., 2004. Stochastic gene expression in fluctuating environments. Genetics 167, 523–530.
Veening, J.W., Igoshin, O.A., Eijlander, R.T., Nijland, R., Hamoen, L.W., Kuipers, O.P., 2008a. Transient heterogeneity in extracellular protease production by Bacillus subtilis. Mol. Syst. Biol. 4, 184.
Veening, J.W., Smits, W.K., Kuipers, O.P., 2008b. Bistability, epigenetics, and bet-hedging in bacteria. Annu. Rev. Microbiol. 62, 193–210.
Vega-Palas, M.A., MartÃn-Figueroa, E., Florencio, F.J., 2000. Telomeric silencing of a natural subtelomeric gene. Mol. Gen. Genet. 263, 287–291.
Webb, J.S., Givskov, M., Kjelleberg, S., 2003. Bacterial biofilms: prokaryotic adventures in multicellularity. Curr. Opin. Microbiol. 6, 578–585.
West, S.A., Buckling, A., 2003. Cooperation, virulence and siderophore production in bacterial parasites. Proc. R. Soc. Lond. B Biol. Sci. 270, 37–44.
West, S.A., Griffin, A.S., Gardner, A., Diggle, S.P., 2006. Social evolution theory for microorganisms. Nat. Rev. Microbiol. 4, 597–607.
Wolf, D.M., Vazirani, V.V., Arkin, A.P., 2005. Diversity in times of adversity: probabilistic strategies in microbial survival games. J. Theor. Biol. 234, 227–253.